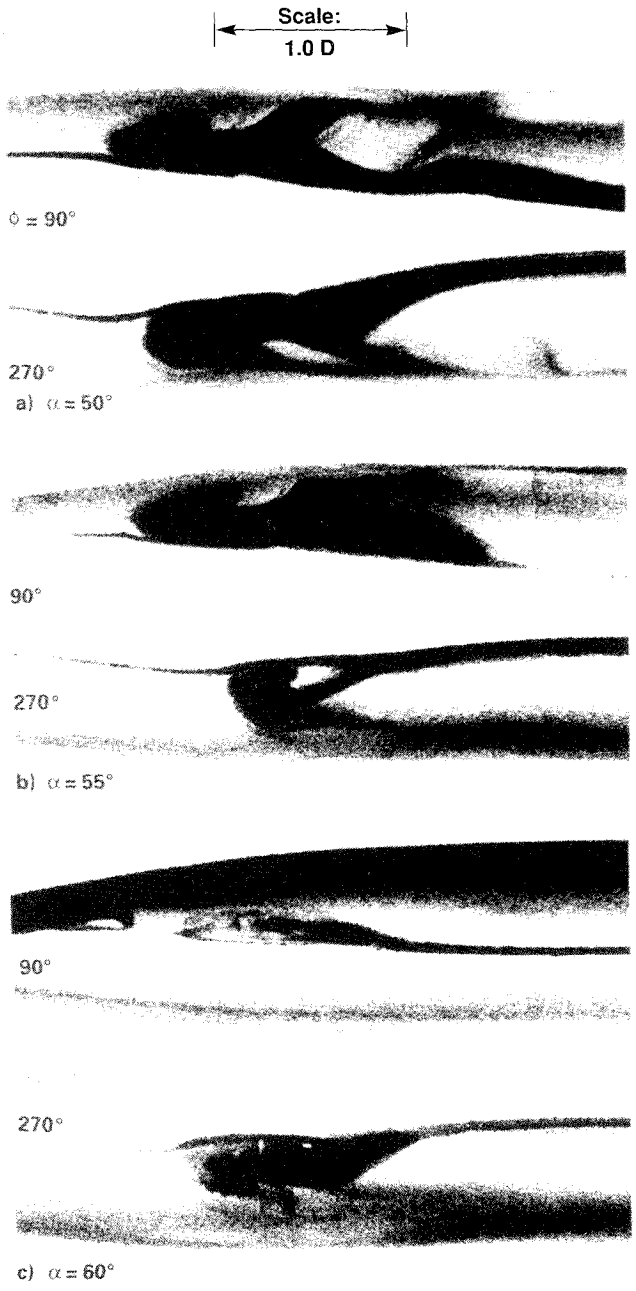

Fig. 2 Details of foci on an ogive cylinder: $Re_D = 2.6 \times 10^4$.

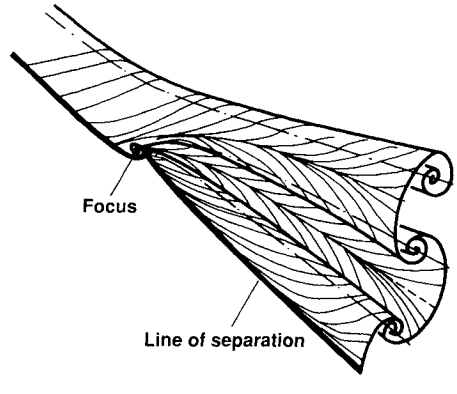

Fig. 3 Conjectured mechanism for formation of trailing-vortex system on an ogive cylinder.

under turbulent flow conditions). If it does, this will be evidence that the crossflow separation on a slender body at incidence has become a regular three-dimensional separation, which will pose a more difficult problem for computational simulation.

References

[1]Hunt, B. L., "Asymmetric Vortex Wakes on Slender Bodies," AIAA Paper 82-1336, Aug. 1982.

[2]Ericsson, L. E., and Reding, J. P., "Aerodynamic Effects of Asymmetric Vortex Shedding from Slender Bodies," AIAA Paper 85-1797, Aug. 1985.

[3]Lamont, P. J., "Pressures Around an Inclined Ogive-Cylinder with Laminar, Transitional, or Turbulent Separation," *AIAA Journal,* Vol. 20, No. 11, 1982, pp. 1492–1499.

[4]Degani, D., and Zilliac, G. G., "An Experimental Study of the Nonsteady Asymmetric Flow Around an Ogive-Cylinder at Incidence," *AIAA Journal,* Vol. 28, No. 4, 1990, pp. 642–649.

[5]Zilliac, G. G., Degani, D., and Tobak, M., "Asymmetric Vortices on a Slender Body of Revolution," *AIAA Journal,* Vol. 29, No. 5, pp. 667–675.

[6]Dexter, P. C., and Hunt, B. L., "The Effects of Roll Angle on the Flow Over a Slender Body of Revolution at High Angle of Attack," AIAA Paper 81-0358, Jan. 1981.

[7]Moskovitz, C. A., Hall, R. M., and DeJarnette, F. R., "Effects of Nose Bluntness, Roughness and Surface Perturbations on the Asymmetric Flow Past Slender Bodies at Large Angles of Attack," AIAA Paper 88-2236, Aug. 1989.

[8]Tobak, M., Degani, D., and Zilliac, G. G., "Analytical Study of the Origin and Behavior of Asymmetric Vortices," NASA TM-102796, April 1990.

[9]Chapman, G. T., "Topological Classification of Flow Separation on Three-Dimensional Bodies," AIAA Paper 86-0485, Jan. 1986.

Interaction of a Planar Shock Wave with a Double-Wedge-Like Structure

G. Ben-Dor*
Ben-Gurion University of the Negev,
Beer Sheva, Israel

Introduction

THE reflection of a planar shock wave over a double wedge is a relatively new topic of research initiated a few years ago by Ben-Dor et al.[1] In their study they established that, for a given incident shock wave Mach number M_i, there are seven different domains of reflection processes in the (θ_w^1, θ_w^2) plane, where θ_w^1 and θ_w^2 are the angles of the first and second surfaces of the double wedge. The inclination of the second surface with respect to the first one is $\Delta\theta_w = \theta_w^2 - \theta_w^1$. Schematical drawings of a concave and convex double wedge are shown at the bottom of Fig. 1.

The seven domains of the different types of the reflection process of a planar shock wave over a double wedge in the (θ_w^1, θ_w^2) plane are shown in Fig. 1. The line $\Delta\theta_w = 0$ divides the (θ_w^1, θ_w^2) plane into the domains of a concave double wedge $(\Delta\theta_w > 0)$ and a convex double wedge $(\Delta\theta_w < 0)$. The line $\theta_w^1 = \theta_w^{tr}|_{M_i}$ (where $\theta_w^{tr}|_{M_i}$ is the RR↔MR transition wedge angle appropriate to the incident shock wave Mach number M_i) determines the initial type of reflection over the first surface. If $\theta_w^1 < \theta_w^{tr}|_{M_i}$, then the shock wave reflects over the first surface as a Mach reflection (MR), and if $\theta_w^1 > \theta_w^{tr}|_{M_i}$, then the reflection of the shock wave over the first surface is regular (RR). The line $\theta_w^2 = \theta_w^{tr}|_{M_i}$ determines the type of the reflection that is

Received July 31, 1990; revision received Oct. 10, 1990; accepted for publication Oct. 10, 1990.

*Department of Mechanical Engineering, Pearlstone Center for Aeronautical Engineering Studies.

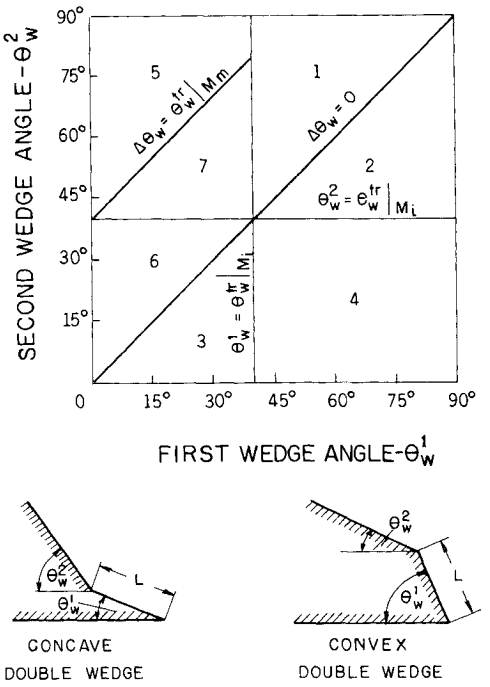

Fig. 1 Domains and boundaries of different types of reflection processes of a planar shock wave (M_i = 1.3) over a double wedge.

finally obtained over the second surface. The final reflection is MR if $\theta_w^2 < \theta_w^{tr}|_{M_i}$, whereas it is RR when $\theta_w^2 > \theta_w^{tr}|_{M_i}$. If the double wedge is concave (i.e., $\Delta\theta_w > 0$) and if the initial reflection over the first surface is MR (i.e., $\theta_w^1 < \theta_w^{tr}|_{M_i}$), then the Mach stem of this MR reflects over the second surface, either as an MR if $\Delta\theta_w < \theta_w^{tr}|_{M_m}$, or as an RR if $\Delta\theta_w > \theta_w^{tr}|_{M_m}$, where $\theta_w^{tr}|_{M_m}$ is the RR↔MR transition wedge angle appropriate to the Mach stem Mach number M_m. It is important to note that M_m is always $> M_i$. However, the RR↔MR transition wedge angle depends very slightly on the shock wave Mach number. For most Mach numbers it is quite practical to assume that $\theta_w^{tr}|_{M_i} \approx \theta_w^{tr}|_{M_m}$. The foregoing discussion regarding the various types of reflection processes of a planar shock wave over a concave or a convex double wedge is summarized in Table 1.

The study of Ben-Dor et al.[1] was aimed at establishing the domains and boundaries of the various types of the reflection processes of a planar shock wave over a concave or a convex double wedge in the (θ_w^1, θ_w^2) plane. The need to understand this phenomenon is quite obvious if one realizes that the discussed reflection processes can take place when a ground explosion generated blast wave interacts with a man-made surface that has a shape similar to that of a double wedge. Consider Fig. 2a where a semispherical blast wave, generated by a ground explosion, is seen to be propagating outwards from the explosion center. Two man-made structures having shapes of a double wedge, one concave and one convex, are added to Fig. 2a on the left and right sides of the blast wave, respectively. If these structures are located far enough from the explosion center, then the portions of the blast wave,

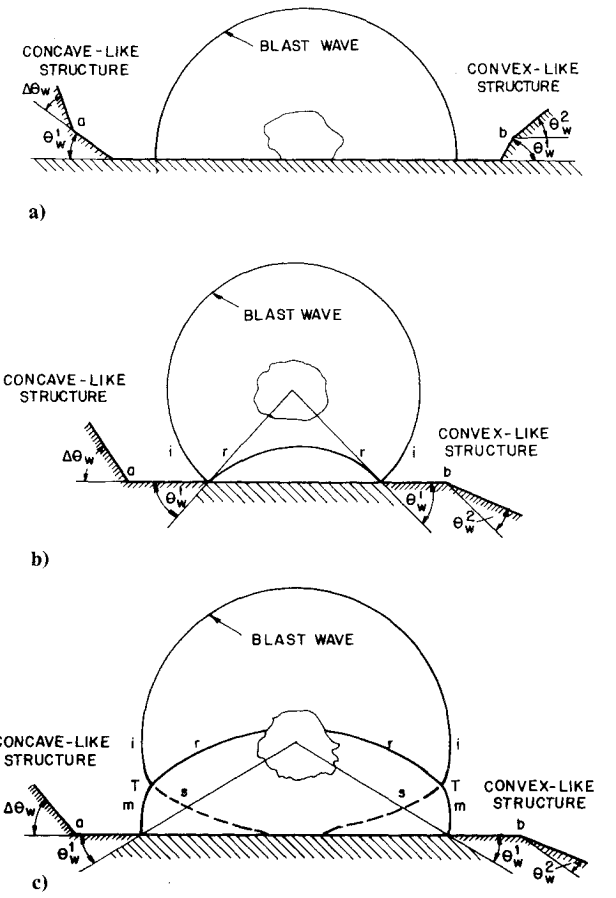

Fig. 2 Schematical illustrations of blast waves experiencing a double-wedge-like interaction: a) semispherical; b) and c) spherical.

which collide with these structures and interact with them, could be considered to be planar. Thus, the reflection processes occurring upon the collision of the blast wave with these two structures is analogous to those over the double wedges just discussed.

If, however, the explosion occurs at some height above the ground, the interaction of the explosion generated spherical blast wave with the ground surface produces an RR, which changes later to an MR. If these reflections collide with man-made structures having the shapes shown in Figs. 2b and 2c, then this reflection phenomenon is again similar to that mentioned earlier (i.e., the reflection of a planar shock wave over a double wedge). Consider Figs. 2b and 2c, where an RR and an MR (resulted from an above-the-ground explosion) are seen to propagate toward the man-made structures. The ground surface, in these cases, could be considered to be analogous to the first surface of the double wedge, and the man-made structures provide the second surface.

In a recent study Itoh et al.[2] reported on a numerical code, based on the upwind total variation diminishing (TVD) scheme, which was originally developed by Harten[3] and later improved by Yee.[4] The code was applied by Itoh[5] to simulate

Table 1 Summary of the seven different reflection processes that can occur over a concave or a convex double wedge

Type of wedge	θ_w^1	θ_w^2	$\Delta\theta_w$	Reflection over first surface	Reflection over second surface	Domains in Fig. 1
Concave double wedge	$>\theta_w^{tr}$	$>\theta_w^{tr}$	—	RR	RR	1
	$<\theta_w^{tr}$	$>\theta_w^{tr}$	$>\theta_w^{tr}$	MR	RR→RR	5
	$<\theta_w^{tr}$	$>\theta_w^{tr}$	$<\theta_w^{tr}$	MR	MR→RR	7
	$<\theta_w^{tr}$	$<\theta_w^{tr}$	$<\theta_w^{tr}$	MR	MR→MR	6
Convex double wedge	$>\theta_w^{tr}$	$>\theta_w^{tr}$	—	RR	RR	2
	$>\theta_w^{tr}$	$<\theta_w^{tr}$	—	RR	MR	4
	$<\theta_w^{tr}$	$<\theta_w^{tr}$	—	MR	MR	3

Table 2 Details of the experiment

Type of wedge	Exp. no.	Domain in Fig. 1	θ_w^1, deg	θ_w^2, deg	M_i	P_0, KPa
Concave double wedge	1	6	15	35	2.16	50.7
	2	7	20	55	2.16	30.4
	3	1	55	75	1.95	50.7
Convex double wedge	4	4	60	30	2.16	30.4
	5	3	35	15	1.49	66.7
	6	2	65	50	1.47	80.0

the reflection phenomenon of a planar shock wave over a concave or a convex double wedge.

Actual experiments, with the initial conditions listed in Table 2, were numerically simulated. The comparison between the numerically predicted contours of constant density and those recorded actually using holographic interferometry, indicated that the numerical code developed by Itoh[5] was capable of accurately simulating these complex flow patterns.

The aforementioned computer code was used by us to obtain the pressure distribution along the surfaces of the double wedge for the various types of reflection processes discussed earlier and summarized in Table 1.

Results and Discussion

Table 2 summarizes the initial conditions of the various reflection processes that will now be discussed. They cover six of the seven domains of different types of reflection processes, which are illustrated in Fig. 1. The pressure distributions along the two surfaces of the various double wedges are given in Figs. 3 and 4. The pressures P are normalized by the ambient pressure ahead of the incident shock wave P_0, and the length along the reflecting surfaces x is normalized by the distance between the leading edges of the two surfaces L (see Fig. 1). The location of the two leading edges are marked with arrow heads at $x/L = 0$ and 1.

Figures 3a–c, which correspond to the reflection over concave double wedges, indicate that the highest pressures are obtained in the vicinity of the leading edge of the second wedge. The pressure peaks there are about 34, 52, and 42% higher than those obtained immediately behind the corresponding incident shock waves or Mach stems. Note that for experiments 1 and 2, in which the final reflection over the second wedge is an MR, the pressure also peaks in the vicinity of the location where the slipstream meets the wedge surface. The pressure peaks there are about 11 and 38% higher than those obtained immediately behind the incident shock fronts. It is also interesting to note that in experiments 1 and 2 there are also pressure peaks near the leading edge of the first

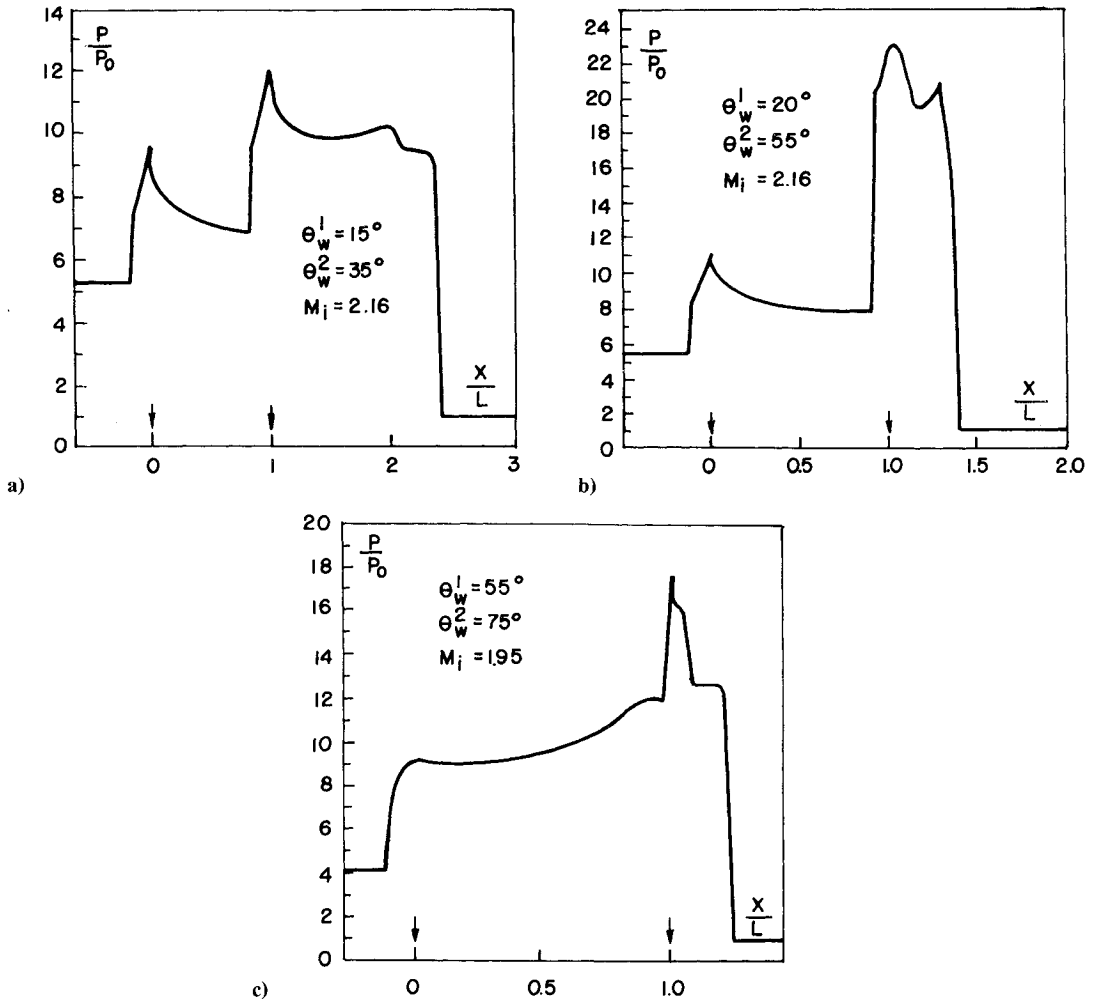

Fig. 3 The pressure distribution along a concave double wedge with a) $\theta_w^1 = 15$ deg, $\theta_w^2 = 35$ deg, and $M_i = 2.16$; b) $\theta_w^1 = 20$ deg, $\theta_w^2 = 55$ deg, and $M_i = 2.16$; and c) $\theta_w^1 = 55$ deg, $\theta_w^2 = 75$ deg, and $M_i = 1.95$.

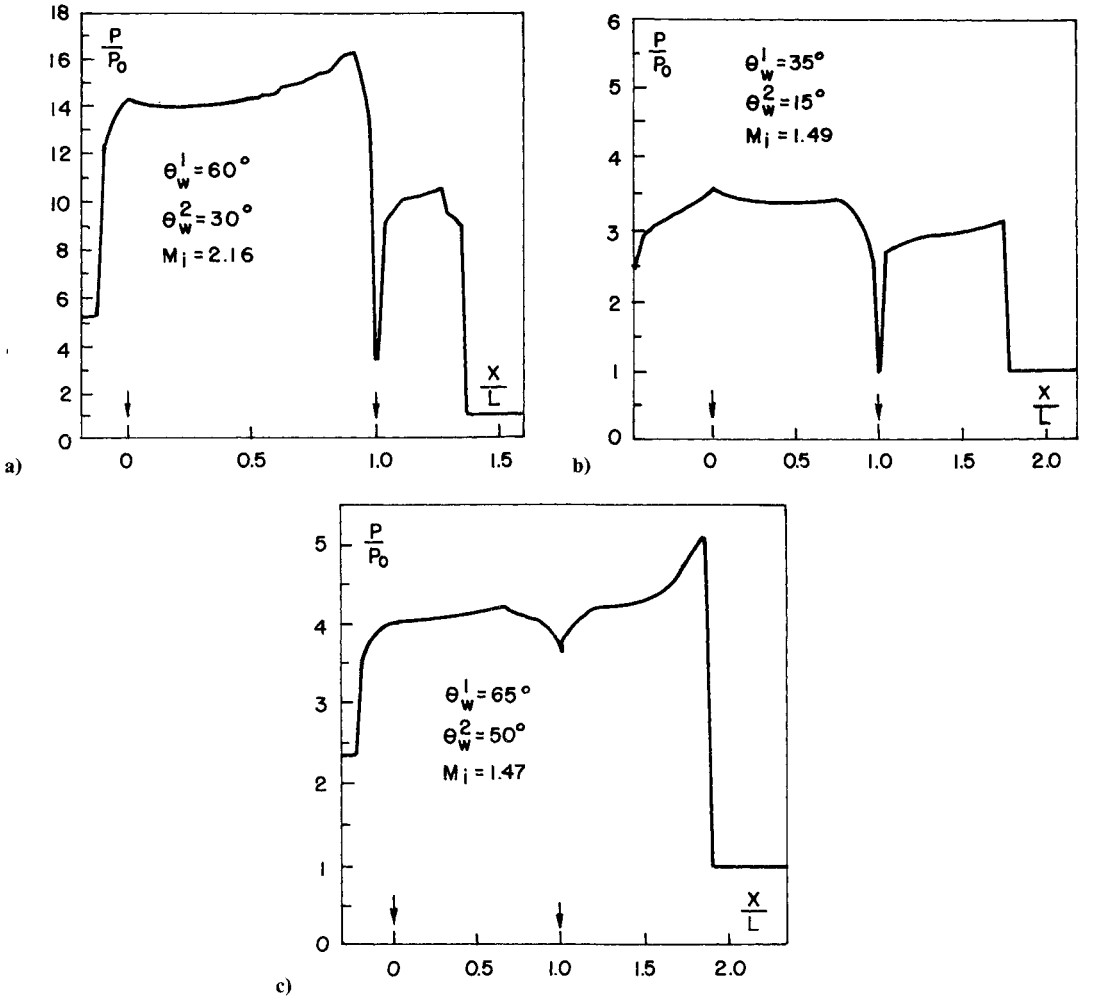

Fig. 4 The pressure distribution along a convex double wedge with a) $\theta_w^1 = 60$ deg, $\theta_w^2 = 30$ deg, and $M_i = 2.16$; b) $\theta_w^1 = 35$ deg, $\theta_w^2 = 15$ deg, and $M_i = 1.49$; and c) $\theta_w^1 = 65$ deg, $\theta_w^2 = 50$ deg, and $M_i = 1.47$.

surface. Following these pressure peaks, the pressure seems to be dropping exponentially along the first surface until the flow encounters the shock wave which reflects from the leading edge of the second surface. At that point a sudden increase in the pressure is noticed. Unlike these two experiments, in experiment 3, where the final reflection over the second surface is an RR, the pressure along the first surface is increasing exponentially until it peaks near the leading edge of the second surface.

The foregoing discussion implies that the highest pressure load on the concave-like structures shown in Figs. 2a-2c is obtained at the point indicated by the letter "a." These points should be designed to withstand the highest pressure load during the interaction of the blast wave with the structure.

When the planar shock wave reflects over convex double wedges (Figs. 4a-4c), an opposite phenomenon is evident. Figures 4a-4c indicate that the pressure drops at the leading edge of the second surface. The pressure in the vicinity of the leading edge of the second surfaces are 29, 0, and 63% of the pressures obtained behind the corresponding incident shock waves, or Mach stems. Note that in Fig. 4b the pressure drops down to the ambient pressure. Thus when the structure is convex-like, the points labeled with the letter "b" in Figs. 2a-c experience the lowest pressure load during the reflection process. Note also that for the cases shown in Figs. 4a and 4b, where the final reflection over the second surface is an MR, the pressure along the two surfaces seems to be quite constant. This is not the case when the final reflection over the second surface is an RR. In this case (Fig. 4c), the pressure along the second surface seems to be dropping exponentially, from a peak pressure immediately behind the reflection point of the RR toward the sharp decrease near the leading edge of the second surface. Along the first surface, however, again an almost constant pressure is obtained.

Finally it should be noted that similar profiles of all the other flow properties could be obtained using the numerical code developed by Itoh.[5]

Conclusions

A numerical code, based on the upwind TVD scheme, capable of simulating the reflection process of a planar shock wave over concave and convex double wedges, was used to numerically investigate the pressure distributions along the two surfaces of the double wedge. The investigation revealed the points along the double wedge that are subjected to the highest and lowest pressures.

Our study was aimed at generally investigating the pressure distribution over double wedges, therefore, available experiments were simulated. For other positions of the incident shock wave over the double wedge, the pressure values would be different. However, based on our findings, there is little doubt about the locations along the doubles wedges where the pressure reaches its maximum or minimum value.

The developed numerical code can be used to investigate the pressure load on man-made structures that have a geometrical shape of a convex or a concave double wedge and are hit by a blast wave.

Acknowledgments

The author would like to thank K. Takayama and K. Itoh from the Shock Wave Research Center, Institute of Fluid

Sciences, Tohoku University, Sendai, Japan, for their support and encouragement throughout this investigation.

References

[1]Ben-Dor, G., Dewey, J. M., and Takayama, K., "The Reflection of a Planar Shock Wave Over a Double Wedge," *Journal of Fluid Mechanics,* Vol. 176, 1987, pp. 483–520.

[2]Itoh, K., Takayama, K., and Ben-Dor, G., "Numerical Simulation of the Reflection of a Planar Shock Wave over a Double Wedge," *International Journal for Numerical Methods in Fluids* (to be published).

[3]Harten, A., "High Resolution Schemes for Hyperbolic Conservation Laws," *Journal of Computational Physics,* Vol. 49, 1983, pp. 357–393.

[4]Yee, H. C., "A Class of High Resolution Explicit and Implicit Shock-Capturing Methods," NASA TN 101088, 1989.

[5]Itoh, K., "Numerical and Experimental Study of Transonic Shock Tube Flows," Ph.D. Dissertation, Inst. of Fluid Science, Tohoku Univ., Sendai, Japan, 1988.

Simple Method of Supersonic Flow Visualization Using Smoke

L. S. Miller* and E. Irani†
Wichita State University, Wichita, Kansas 67208

Introduction

DIRECT smoke injection is a common and popular means for studying aerodynamic phenomena in wind tunnels. A number of smoke flow-visualization techniques currently exist and are used depending on the desired test information, available facilities, available smoke-generation apparatus, and test flow speeds.

Smoke visualization may be conducted in virtually any type wind tunnel. However, a good visualization tunnel will typically utilize a large contraction ratio inlet and inlet face screens and honeycomb to improve flow stability, reduce turbulence scales and flow angularity. These features reduce the likelihood that the injected smoke will dissipate before important model aerodynamic features can be observed.

A number of different smoke-generation techniques are available, each varying in capability and complexity. An overview of methods is provided by Mueller.[1] A common approach involves heating a glycol solution to produce a smoke-like vapor cloud, which is pumped to a rake assembly positioned at the wind-tunnel inlet. About 1–20 smoke filaments can be introduced into a flow in this fashion. This visualization method works well over a range of test speeds and has been demonstrated at supersonic speeds.[2] Although popular and successful, this technique has some disadvantages. The generator and rake assemblies are relatively complicated to build and must be carefully maintained to insure proper operation. In addition, a greater number of smoke filaments may be desirable to improve flow-feature visibility.

The smoke wire method overcomes some smoke-rake problems and has provided spectacular images at low flow speeds. The technique relies on a small 0.025–0.125 mm diam wire for smoke filament generation.[3] The wire, positioned in the wind-tunnel test section upstream of the model, is coated by an oil film and heated for a short period of time electrically. Heating causes the oil to vaporize, generating a large number of smoke filaments (typically 5–10 per cm). It is the method's simplicity and the large number of fine filaments generated which are particularly attractive. Unfortunately, at wire Reynolds numbers above 40, an unsteady wake develops which dissipates the smoke filaments and reduces visualization quality.[3] This Reynolds-number constraint limits tunnel test section speeds typically to less than 10 m/s. In addition, since the wire diameter is small, the amount of smoke produced and the generation duration are limited. This problem can place special demands on the experimentalist for photography.

Received Sept. 11, 1990; revision received Feb. 7, 1991; accepted for publication Feb. 22, 1991.

*Assistant Professor, Department of Aerospace Engineering. Member AIAA.

†Research Assistant, Department of Aerospace Engineering. Member AIAA.

Alternative Method

A modified smoke wire visualization method for application in high-speed and supersonic flows has been developed which produces a large number of fine smoke filaments that do not dissipate. The principal difference between the new technique and the low-Reynolds-number method discussed earlier is related to the diameter and placement of the smoke-generation wire. The wire diameter has been notably increased and it is now positioned at the wind-tunnel inlet face, instead of inside the test section. Higher test section flow speeds, with excellent visualization, are achieved since the inlet-wire Reynolds number is smaller than the corresponding test section value. Also, interestingly, a greater Reynolds number can be tolerated since the inlet contraction, screens, and honeycomb damp out or reduce unsteady smoke flow from the wire and preserve smoke-filament quality during transit to the test section. In addition, the large-diameter wire is capable of holding more oil and can thus produce smoke for a longer period of time.

Facility, Apparatus, and Procedure

A 0.1 × 0.1-m vacuum induction-type wind tunnel, operating at Mach 2 flow speed, was used for method development and demonstration. Ten layers of common window screen and a single layer of 5-mm cell honeycomb are installed on the tunnel inlet, which has an area contraction ratio of 100:1. A 1.5-mm-diam stainless-steel tube installed vertically, approximately 15 mm upstream from the tunnel inlet, was used to generate smoke (see Fig. 1). By using a tube, as opposed to a solid wire, less current is required for a necessary amount of heating. The wire was kept in tension during runs by a spring to assure that bending due to thermal expansion would not occur.

Glycol or model-train smoke oil, applied with an eye dropper, was used as a fuel for smoke generation. "Life-Like Train Smoke" oil and about 10 amperes of current was found to generate the best quality and longest duration smoke filaments. Around 5–10 smoke filaments per centimeter are produced for 2–4 s.

A conventional 35-mm camera and black-and-white film were utilized to record the visualization results. A motor drive and remote shutter release were fitted to the camera to allow ease of operation and rapid photography as desired. A range of film speeds was examined for use, but 400 ASA film was primarily employed.

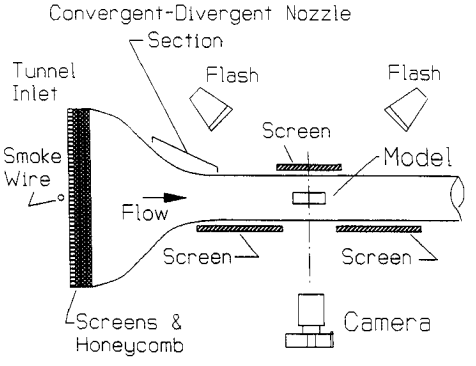

Fig. 1 Top view of experimental setup and supersonic wind tunnel.